Mechanisms for Chemical Vapor Deposition Carbon Nanotube Growth by Surface Modification of 316L Stainless Steel

Joshua Hancock

A senior thesis submitted to the faculty of
Brigham Young University
in partial fulfillment of the requirements for the degree of

Bachelor of Science

Richard Vanfleet and Felipe Rivera, Advisors

Department of Physics and Astronomy

Brigham Young University

ABSTRACT

Mechanisms for Chemical Vapor Deposition Carbon Nanotube Growth by Surface Modification of 316L Stainless Steel

Joshua Hancock
Department of Physics and Astronomy, BYU
Bachelor of Science

The scope of this research is to analyze and attempt to model the mechanisms responsible for carbon nanotube growth on a stainless steel substrate. CNTs were grown on 316L steel samples by first exposing the surface to air at high temperatures to build up an oxide layer. This treated steel was then exposed to ethylene gas at the same temperature, which promoted CNT growth on the substrate. The oxides of some samples were reduced with hydrogen prior to CNT growth by ethylene. At 800 °C, pre-growth reduction was found to inhibit significant CNT growth. At 700 °C, CNTs yield was less affected by pre-growth reduction, and the CNTs produced were found to have smaller diameters than those without pre-growth reduction. The CNTs had a multi-walled structure and an average diameter of 39 nm. Samples grown at 800 °C were analyzed using both Scanning and Transmission Electron Microscopy to characterize how the growth process modified the steel surface. Iron-rich nanoparticles were seen in the tips, cores, and bases of the CNTs. X-Ray spectroscopy was used to show that iron left the oxide layer over the course of CNT growth. This suggests that the iron-rich particles were reduced out of the oxide layer during the growth process. These iron-rich nanoparticles acted as the primary catalysts for CNT growth.

Keywords: CNT, stainless steel, annealing, EDX, SEM/TEM, FIB

ACKNOWLEDGMENTS

This research was only possible thanks to the help and support of my advisors, my family, and all the students and staff that worked on this project before me.

I would like to sincerely thank my chief advisor, Dr. Richard Vanfleet, for introducing me to this amazing field of research and helping me to develop the skills and attitudes that made this project possible. He has been both an incredible instructor and an amazing example. I would also like to thank my advisor Dr. Felipe Rivera, whose expertise in microscopy and continuous coaching was invaluable in data collection and interpretation. I would like to thank Dr. Brian Jensen for his advice, perspective, and encouragement during the course of this project. He and his students helped to perform amazing preliminary work that served as the groundwork for this project.

I would like to especially thank the Electron Microscopy facilities here at BYU, whose equipment and staff were essential to the data we collected. I would like to thank Michael Standing in particular for his training and help in using the Helios SEM/FIB. I would also like to thank Paul Minson for helping me to analyze my samples using the Tecnai TEM and for his advice and help on this project. I am especially thankful to these two men and Felipe Rivera for teaching the electron microscopy courses of Physics 586 and 588, which helped me to better develop the skills I used for this project and that I hope to use in a future career in materials science. Without these tools and facilities, projects like these simply wouldn't be possible, and I am grateful to BYU for allowing undergraduates like myself to have access to these incredible microscopes.

Finally, I would like to acknowledge the support I have received from my mother, Michelle, over the course of this project and my education. Though she was unable to complete her own education, she has worked tirelessly to financially support her four children during their times at college. Her example and faith in my success pushed me to strive for the kind of excellence that Brigham Young University expects of its undergraduates.

Contents

Table of Contents **iv**

List of Figures **v**

1 Introduction **1**
1.1 Background 2
1.2 Previous Research at BYU 5
1.3 Thesis Overview 7

2 Methods **8**
2.1 CNT Growth Process on Stainless Steel 8
2.2 SEM Imaging and FIB Cross-Sections 9
2.3 STEM/TEM Imaging and EDX Analysis 12

3 Results and Discussion **14**
3.1 General Characteristics of the CNTs and CNFs 14
3.2 Effects of Temperature and Hydrogen Reduction 18
3.3 Composition of the Steel Surface and Nanoparticles 23
3.4 Conclusions: Model of Growth 32
3.4.1 Oxidizing Heat Treatment 32
3.4.2 Oxide Reduction 32
3.4.3 Short CNT growth 32
3.4.4 Long CNT growth 33
3.5 Future Work 33

Appendix A Sample Key **36**

Bibliography **37**

Index **39**

List of Figures

1.1 Carbon nanotube and carbon nanofiber structures and sizes 2

1.2 Basic CVD process for CNT growth on silicon substrate 3

2.1 Furnace process for CNT growth 10

2.2 Process for creating cross-sections with dual-beam FIB 11

2.3 STEM image of FIB lamella showing the interaction of a CNT with the steel substrate 13

3.1 Example SEM image of CNTs grown on stainless steel substrate 15

3.2 Distribution of CNT diameters from various samples 16

3.3 High magnification SEM image of CNTs with iron nanoparticles in their tips . . . 17

3.4 High resolution TEM image of MWCNT crystal structure and iron nanoparticle . . 17

3.5 High resolution TEM image of imperfections within MWCNTs 18

3.6 Scrape test comparing adhesion between samples grown at 800 °C and 700 °C . . . 19

3.7 Effects of hydrogen reduction on CNT growth at 800 °C vs 700 °C 20

3.8 Plot of CNT growth height for samples grown with different temperatures and reduction lengths 21

3.9 Plots of CNT diameters with and without pre-growth hydrogen reduction 22

3.10 EDX spectra of TEM lamella, comparing composition of oxide against steel bulk. . 24

3.11 EDX spectra comparing oxide composition over course of CNT growth 26

3.12 EDX spectra comparing oxide composition over course of CNT growth 27

3.13 EDX spectra of regions in cross-section of 3-minute growth sample 28

3.14 Colorized regions in cross-section of 3-minute growth sample 29

3.15 EDX spectra of regions in cross-section of 15-minute growth sample 30

3.16 Colorized regions in cross-section of 15-minute growth sample 31

3.17 Illustrated model for CNT growth on stainless steel 34

Chapter 1

Introduction

Due to their unique chemical and physical properties, carbon nanotubes (CNT) are an attractive nanomaterial for various applications. For example, CNTs can be used as an additive to cement and concrete in order to improve the compressive strength, tensile strength, electrical conductivity, and bonding strength of the material [1]. CNTs also have a variety of potential applications in electronics, optics, and medicine.

In their most basic form CNTs are long tubes made from rolled sheets of graphene. In this form, they are sometimes known as single-walled carbon nanotubes (SWCNT) or multi-walled carbon nanotubes (MWCNT) when they are formed from multiple concentric sheets. Alternative structures also exist, such as conical shells, stacked platelets, or amorphous structures; which are often collectively referred to as carbon nanofibers (CNF). Various CNT structures can be seen illustrated in Figure 1.1.

There are many techniques for CNT and CNF growth, but among the most common is chemical vapor deposition (CVD). In this process, a substrate is first prepared by depositing a barrier layer, followed by a catalyst layer onto the surface. The substrate, barrier, and catalyst materials vary; but a common example is a silicon substrate with an alumina barrier and iron catalyst [3]. This layer deposition may be done by thermal evaporation, magnetron sputtering, or other similar techniques.

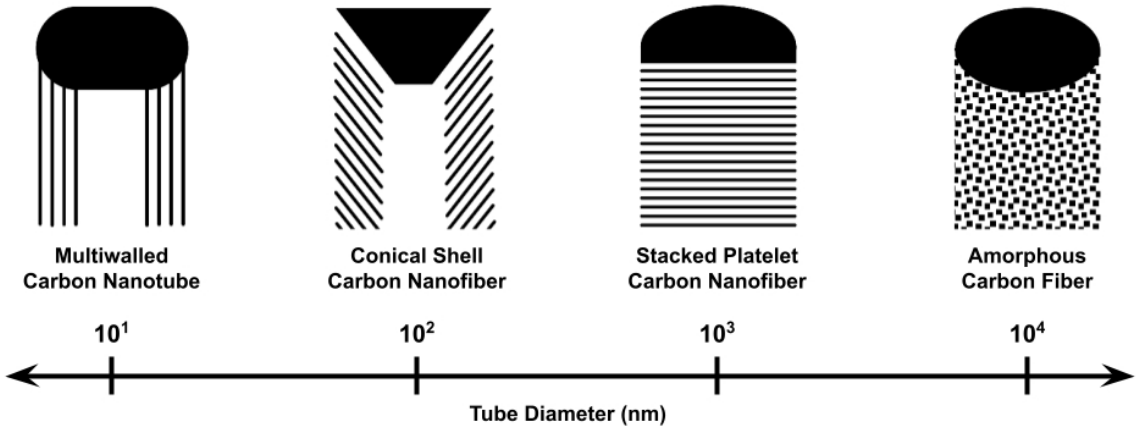

Figure 1.1 Cross-section schematics for various forms of carbon nanotube and carbon nanofiber crystal structures. Each structure tends to have a range of tube diameters, as shown on the axis beneath the image. Adapted from Mori and Suzuki [2].

Unfortunately, the directional nature of many of these deposition techniques means that CNT growth is generally restricted to flat substrates. Figure 1.2 illustrates the process of CVD growth on a silicon substrate.

Stainless steel stands out as a unique choice of substrate because it may not require additional catalysts to grow CNTs [4]. As a result, samples can be prepared for CNT growth without depositing any additional layers. This means that CNTs may grow on contoured surfaces, and samples may be prepared with fewer steps and equipment. For these reasons, stainless steel has the potential to be a simpler and possibly more effective CNT substrate for making bulk CNTs or CNT coatings than traditional substrates.

1.1 Background

Due to its unique properties as a substrate, various groups have researched stainless steel-grown CNTs over the last decade. In general, it has been seen that CNTs can be grown on stainless steel

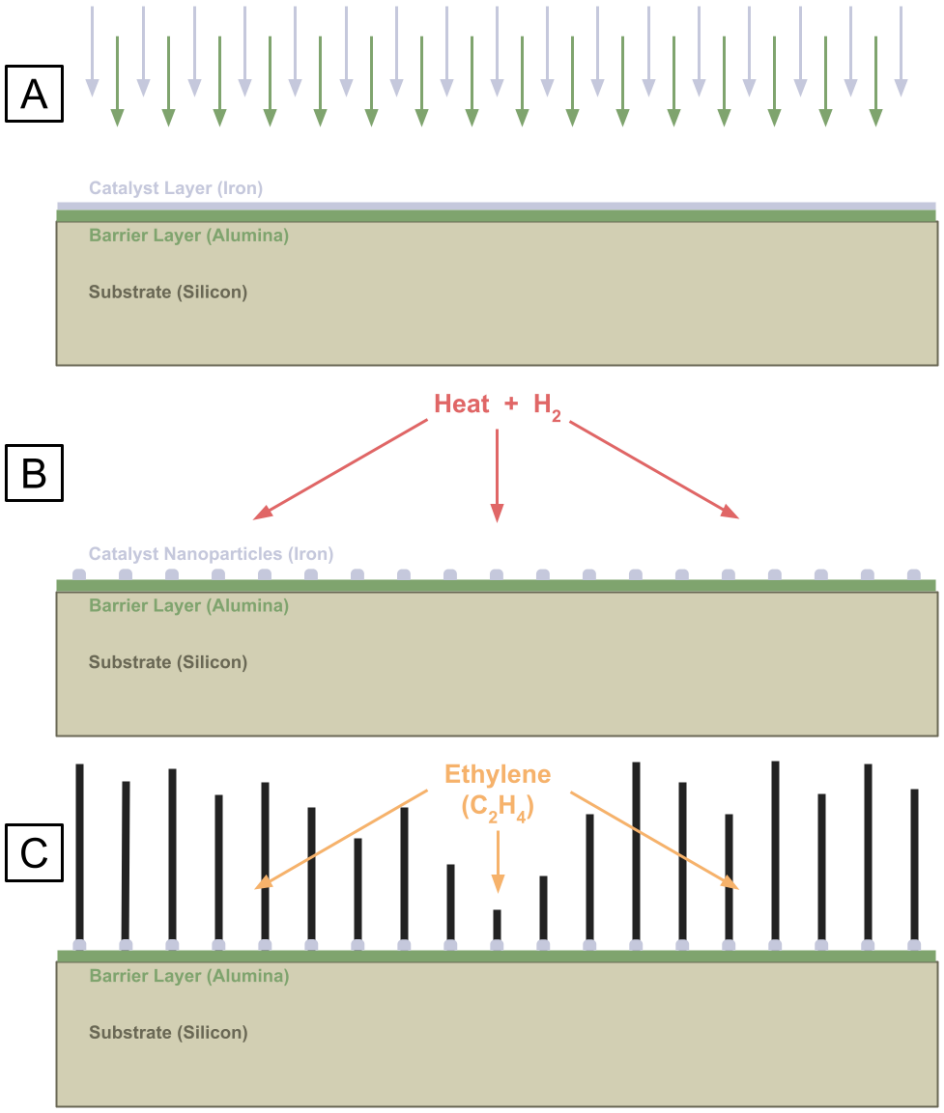

Figure 1.2 Illustration of a basic CVD process for CNT growth on silicon. A) The substrate is prepared by having a an alumina barrier layer and a thin iron film deposited onto the surface. B) The sample is heated to break the iron layer into small nanoparticles, and hydrogen gas is used to reduce any oxides present on the particles before growth. C) Hydrocarbon gas, such as ethylene, is flowed over the sample at high temperatures. The iron nanoparticles help to break down the ethylene into carbon and hydrogen, catalyzing the growth of the nanotubes.

alloys without depositing additional barrier or catalyst layers. Without the directional constraints of layer deposition, CNTs have been successfully grown on steel foils, wire meshes, tubes, pins, and sheets. In this section, the key results and claims of various researchers will be discussed.

Camilli et al. (2011) found that acetylene gas could be used to grow MWCNTs on oxidized steel when heated to 730 °C [5]. They observed iron particles present in the tips and at the bases of the nanotubes, which they believed served as the seed particles for CNT growth [6]. Camilli was uncertain of the process that pulls these iron particles out of the steel.

Zhuo et al. (2014) grew their CNTs on a 316L stainless steel wire mesh. To modify the surface of the steel in preparation for CNT growth, the surface was given an oxidizing heat treatment in air at 800 °C, before ethylene was used to grow CNTs at 800 °C. The time of this treatment varied, but it was found that shorter heat treatments (under 5 minutes) produced the highest CNT yield. It was seen by SEM imaging that heat treatment creates a faceted oxide layer on the steel surface, which is thicker and rougher with longer heat treatments. Zhuo believes that the iron nanoparticle catalysts are being reduced out of this oxide layer during the growth process [7].

Pattinson et al. (2015) used a stainless steel mesh in an attempt to produce large amounts of CNTs.They prepared their steel surface via a heat treatment in air prior to growth, testing various heat treatment temperatures. High temperature anneals were shown to increase CNT yield dramatically, and nanotubes were observed to have iron-rich nanoparticles as tip-based catalysts [8].

Padkee et al. (2017) grew CNTs on 304 stainless steel foil using active temperatures ranging from 600 to 900 °C. They found that CNT diamter generally decreased with increasing temperature, and no CNTs grew at 900 °C. Instead, large amorphous carbon nodules grew on the surface at this high temperature. By performing Energy Dispersive X-Ray Spectroscopy (EDX) on cross-sections of heat treated steel (see Section 2.2-2.3), Padkee observed that the surface of the steel had less chromium and iron than the deeper bulk. They suspected that these metals left the surface to form the oxide layer, and the missing iron was used to create catalytic nanoparticles for CNT growth [4].

From these four groups, it appears that oxidizing the surface is a key step to preparing the steel for CNT growth. This can be done at a variety of temperatures, but appears to work best at temperatures above 600 °C. CNTs can be grown at temperatures ranging from 600 to 800 °C, and above this range, amorphous growth dominates. Nanotube diameter varies greatly across studies, but most appear to be either MWCNTs or cone shell CNFs, ranging from 20-150 nm in diameter. All groups observed iron nanoparticles inside their nanotubes. As such, the prevailing model is that during CNT growth, these iron particles are pulled out of the oxide layer to act as catalysts.

While various groups have used EDX analysis (See section 2.3) to observe how the composition of the substrate changed at various points in the growth process, all of these were done on the bulk of the material. To better analyze the composition of small regions or layers of the material, we believe that creating lamella cross-sections and analyzing them in a Scanning Transmission Electron Microscope (STEM) will allow us to more carefully monitor the changes in the steel over the growth process (See section 2.3). This technique has been demonstrated successfully in the analysis of carbon nanotube substrates by Ke et al. [9].

1.2 Previous Research at BYU

Previous to the research presented in this thesis, several other students investigated the properties of steel-grown CNTs here at BYU. The results and questions left by these research projects were crucial in establishing the goals and direction of our experiments. They also helped to develop and establish the process for CNT growth that we used in this paper. As such, it is important to review the findings from these students' work.

Among the first motivations for studying steel-grown CNTs here at BYU was as an antimicrobial coating for biomedical implants. Because steel substrates require no deposited layers, CNTs can be grown uniformly on contoured and complex surfaces, such as pins and screws. In addition, CNTs coatings have been shown at BYU to discourage the growth of biofilms due to their structure. For

this purpose, Stephanie Morco (2021) investigated whether stainless steel implants could be made more microbe-resistant by growing CNTs on the surface. Nanofibers were successfully grown on steel fixator pins and hollow pipes. Although the nanofibers were randomly oriented and wide in diameter, they still discouraged biofilm growth on the steel, making this seem like a promising method for medical application [10].

At the same time, Sterling Voss (2021) investigated how the mechanical and chemical properties of the steel were changed by the CNT growth process. He found that CNTs grown on stainless steel had high adhesion, remaining fixed to the surface of a fixator pin even after it was screwed into bone. Unfortunately, steel treated with the CNT growth process was far less resistant to corrosion than control samples. Stainless steel is normally corrosion resistant due to a passive chromium oxide layer that protects the surface. So some part of the CNT growth process may have modified the steel surface such that it can no longer produce this layer effectively. As such, even though the CNTs resisted biofilm growth, rusting of the steel made them unsuitable for use in medical implants [11].

In order to better understand the mechanisms that drive CNT growth on stainless steel, Michael Manwaring (2021) performed STEM and EDX analysis on several samples. During this project, a promising method of growth was established, which allowed us to grow samples quickly at a constant temperature (see Section 2.1). Manwaring found that the oxide layer created during the heat treatment step contained Cr, Fe, and O, but not Ni. After 15 minutes of growth, this oxide layer had been completely reduced to a discontinuous layer of Cr and Fe. This differed from the bulk of the steel, which was composed of Fe, Cr, and Ni. Iron-rich nanoparticles were also seen inside the nanofibers [12].

Several important questions remained from this body of work. Firstly, how were the iron nanoparticles that catalyze CNT growth formed? Secondly, why does the CNT growth process cause the steel to lose its corrosion resistant properties? Answering these questions was a key driving factor for this project.

1.3 Thesis Overview

The primary objective of this thesis is to determine how iron nanoparticles are formed on the stainless steel surface to catalyze CNT growth. In addition, we want to understand how the steps in this process change the surface of the steel to affect its corrosion resistant properties. Furthermore, we want to understand why an oxide layer is important to prepare the steel for CNT growth.

We hypothesize that the oxide layer on the steel is reduced during growth to produce iron catalyst particles. To test this hypothesis, we analyzed how the composition of the oxide layer changed over the course of the CNT growth process. In order to analyze the composition of such a small region, Transmission Electron Microscopy and Energy Dispersive X-Ray Spectroscopy were used on cross-sections of our samples. Our final results include an illustrated model for CNT growth on stainless steel based on our findings.

Chapter 2

Methods

This chapter outlines how we produced and analyzed our CNT samples. The primary techniques used to collect data were forms of electron microscopy. These allowed us to study the form and composition of our nanotubes and stainless steel substrate.

2.1 CNT Growth Process on Stainless Steel

We used type 316L stainless steel plates with a mirror polish finish as our sample substrates. These were cut into small chips, approximately 1 cm x 1 cm. To protect the surface from contamination, the manufacturer's protective film was left on until it was ready for growth.

To prepare the stainless steel surface for CNT growth, the first step was to give the steel an oxidative heat treatment. A gas fed tube furnace was heated up to the active temperature (either 700 or 800 °C) and fed with 370 sccm of regular air. Once the temperature stabilizes, a sample chip is inserted into the furnace on a quartz glass boat. This chip is exposed to the air flow for 4 minutes, during which the surface oxidizes.

When the 4 minutes have passed, we begin to flow 300 sccm of argon gas over the sample and the air flow is switched off. Argon purges the furnace for about 10 seconds, after which we begin to

flow 340 sccm of ethylene in addition to the argon. This ethylene-argon mixture is passed over the sample for a predetermined growth time, which varies from sample to sample, but ranges from 0-30 minutes. CNTs grow on the surface during this process. Once the predetermined growth time has elapsed, the ethylene flow is switched off, leaving only argon flowing through the tube. After this, the furnace is cooled off to 200 °C, after which the sample is removed.

An optional step was added to some samples between the heat treatment and growth steps. This step was a hydrogen reduction, which was used to reduce the oxides built up in the heat treatment before the surface was exposed to ethylene for growth. In this step, the furnace tube is purged with argon, as explained in the growth step, after which 310 sccm of hydrogen is flowed with the argon. This gas mixture is passed over the sample for a time ranging from 0-60 minutes.

A graphic representation of the full process can be seen in Figure 2.1. Certain parameters were varied between the different samples we prepared; such in furnace temperature, reduction time, and growth time; in order to help us draw comparisons as to how each parameter affects the substrate. A detailed listing of the parameters used for each of our samples can be found in Appendix A.

2.2 SEM Imaging and FIB Cross-Sections

The surface of each sample was imaged using a FEI Helios Nanolab 600 Scanning Electron Microscope (SEM). The high resolution of the electron microscope allows us to study the fine surface details of the nanotubes and make length measurements of important features, such as nanotube diameter, growth density, and nanotube growth height. Growth height was measured by focusing on the steel substrate, then the tops of the nanotubes, and comparing the focus lengths. Nanotube diameters were measured from SEM images using ImageJ.

To test CNT adhesion to the substrate, a plastic stylus was used to gently scrape the CNTs off a region of some some samples. These regions were then imaged in SEM to compare how cleanly the CNTs could be removed.

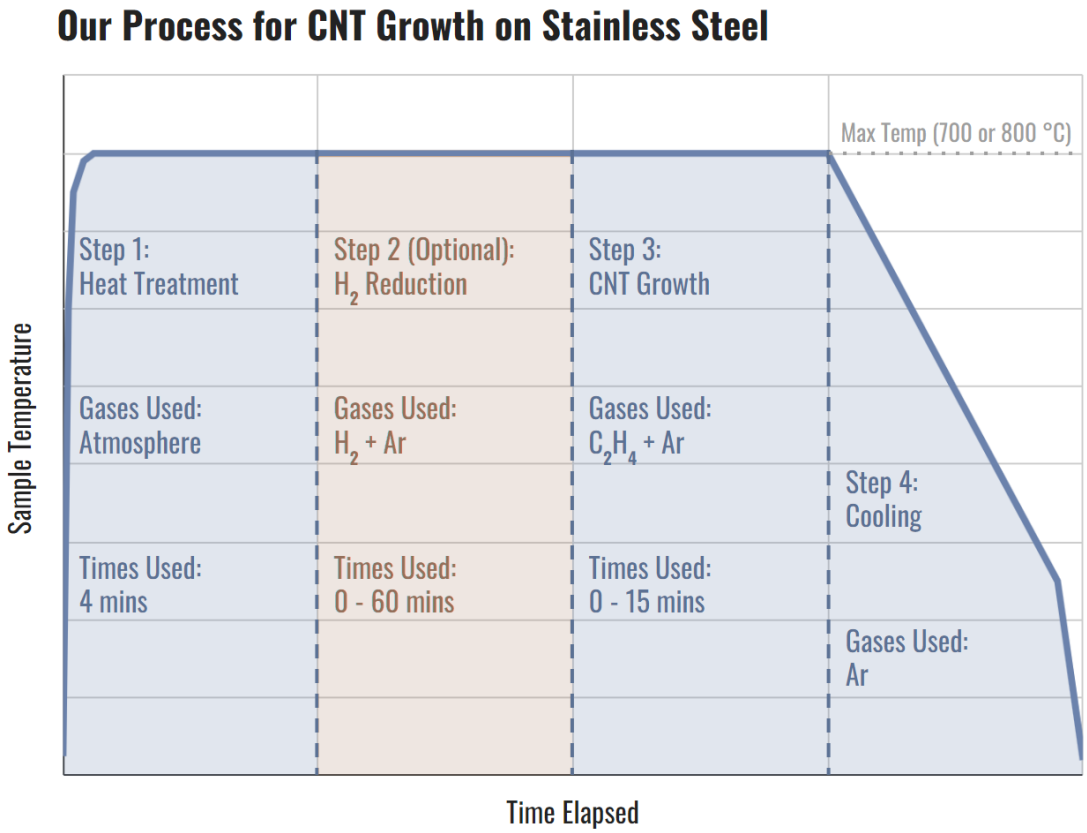

Figure 2.1 The CNT growth process we used can be broken down into four steps: heat treatment, hydrogen reduction, CNT growth, and cooling. The first three steps take place at the same furnace temperature, either 700 or 800 °C depending on the sample. The hydrogen reduction step is optional and was only performed on some samples to better understand how this process affects the steel.

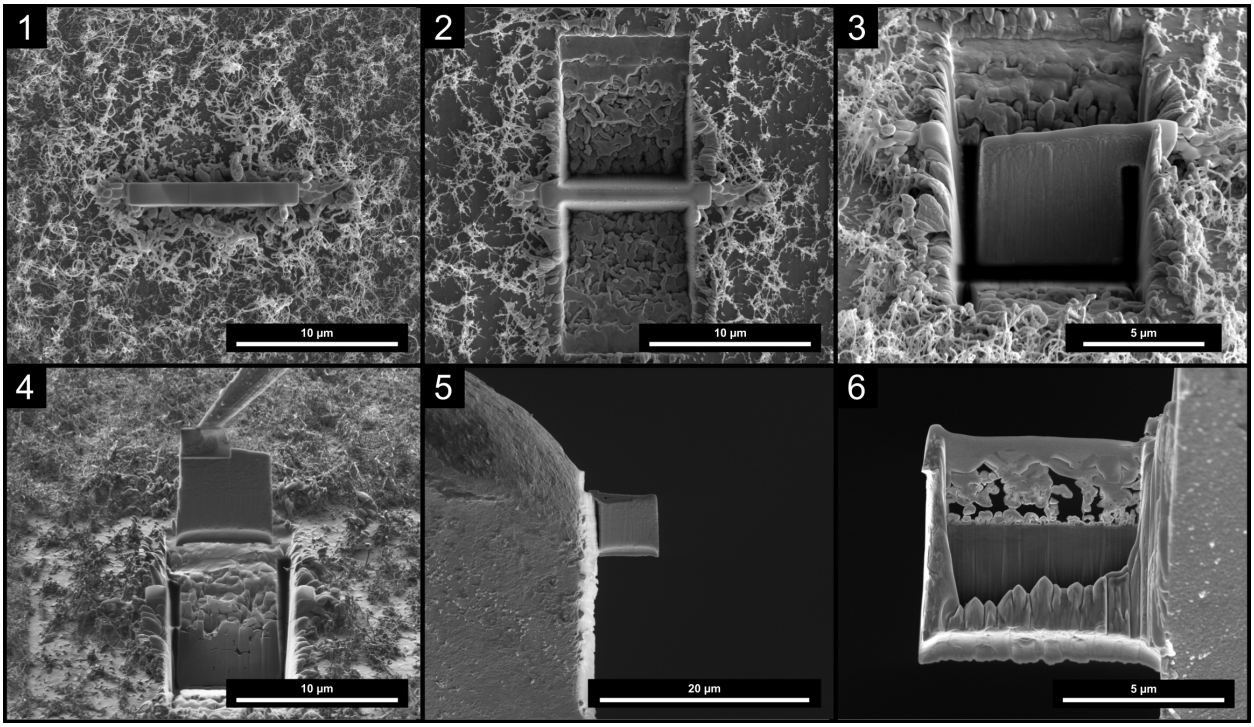

Figure 2.2 This chart depicts a 6 step process we used to create our TEM lamella cross-sections. Our samples were first coated in a 30 nm layer of alumina via ALD to protect the nanotubes while using the FIB. 1) The FIB is used to deposit a rectangular cap of organic-Pt composite on the surface. 2) The FIB is used to mill two regular cross-section cuts on either side of the cap, leaving a bridge. 3) The FIB is used at an angle to mill a "J-cut" around the remaining bridge. 4) An omniprobe needle is brought into contact with the sample and welded on. The connection point left from step 3 is removed, and the sample is lifted out of the hole with the omniprobe. 5) The sample is brought into contact with a TEM copper grid and welded on. After this, the omniprobe needle is removed with the FIB. 6) The FIB is used to carefully thin the cross-section via "cleaning cross-section" cuts. This continues until the sample is <100 nm thick.

To better see how the nanotubes interact with the steel, a Focused Ion Beam (FIB), equipped within the Helios SEM, was used to mill vertical cross-sections into some samples. To prepare the surface for milling, samples were first coated in 20-30 nm of aluminum oxide via atomic layer deposition (ALD). This alumina layer helps to protect the nanotubes from the ion beam during the milling process and also helps to isolate the original material from redeposition (see Figure 2.3). The full process of making these cross-sections is illustrated in Figure 2.2.

2.3 STEM/TEM Imaging and EDX Analysis

To better understand the structure of our produced CNTs, we imaged them in a Transmission Election Microscope (TEM). We used a FEI Tecnai F20 S/TEM to image our samples. CNTs were prepared by scraping them off of the substrate and into isopropyl alcohol. This CNT solution was then placed onto lacey carbon TEM grid and allowed to dry. High resolution TEM imaging of the CNTs allowed us to measure the spacing of lattice planes in the CNTs and their metallic nanoparticles (see Figure 3.4).

As previously stated, thin cross-sections called lamella were made from several chosen samples to be imaged and analyzed in a Scanning Transmission Election Microscope (STEM). Using an annular dark-field detector (ADF) with different camera lengths, we could emphasize different types of contrast within the image. Diffraction contrast allowed us to see the different grains in the oxide and the steel, and Z-contrast allowed us to distinguish which regions of the sample were made from heavier elements. An example of a STEM image of one of our lamella is shown in Figure 2.3.

In addition to imaging, Energy Dispersive X-Ray Spectroscopy (EDX) was used to analyze the element makeup of the sample. As the electron beam scans the sample, it excites native atoms, occasionally knocking out electrons from the sample. This causes the partly ionized atom to undergo several energy transitions that release characteristic X-rays. The energy of these x-rays corresponds to the energy levels of the atoms, allowing us to deduce which elements are present in the sample. Because of the small electron interaction volume in STEM imaging, we can collect x-ray spectra from different spots and compare them to see how the composition varies across the sample.

It is important to note how we compared our EDX data. Because the data relies on number of counts, which can vary depending on thickness, density, exposure time, and other variables; it is vital to normalize the spectra to some chosen value. As such, EDX data is not quite quantitative, but instead can be comparative between regions. Because we were most interested in how the

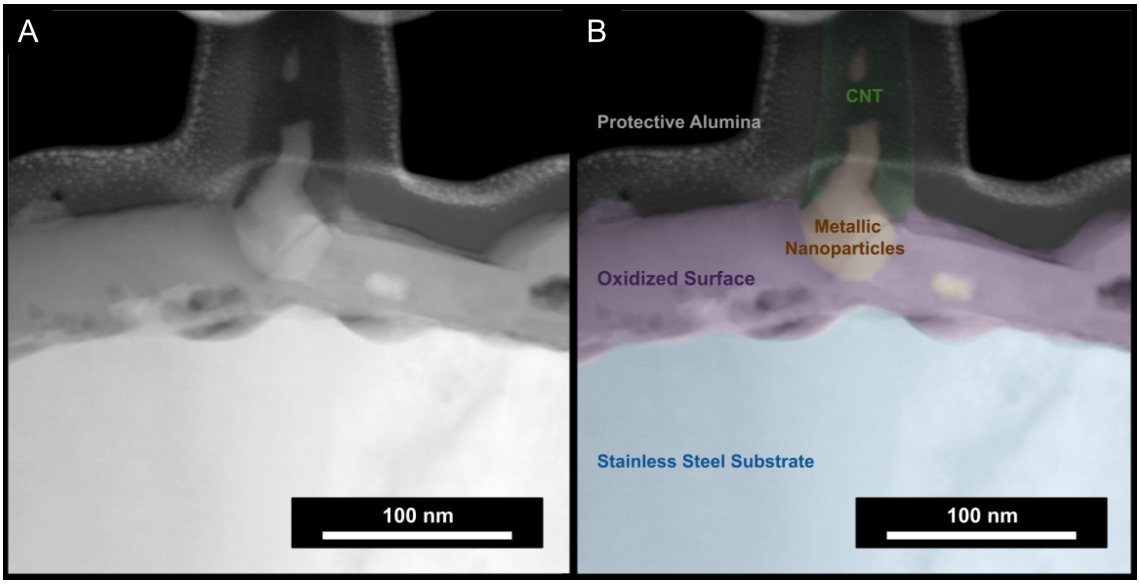

Figure 2.3 This lamella was taken from sample 20 (see Appendix A). A CNT is seen growing off of the oxide layer with a metallic particle at the base. On the right, color contrast has been added to the image to help better distinguish the different regions. The protective alumina layer (uncolored) isolates the original material (colored) from any redeposition, greatly aiding in image interpretation and sample protection.

composition of the steel and its oxide changed, we decided it would be best to normalize most spectra to the Fe Kα peak. By keeping all our normalizations consistent to this peak, it allowed us to compare how the ratio of Fe to other elements changed between samples and regions.

We used EDX to analyze the bulk steel, the oxide surface layer, and metallic nanoparticles seen within the oxide layer and the CNTs. By comparing each region against the bulk steel, we can see how the CNT growth process modified the surface of the steel. By comparing samples with different parameters, we can see how each effects the overall growth process. The results of our EDX analysis is among the most important data we used in forming our final model for CNT growth.

Chapter 3

Results and Discussion

This chapter reviews the observations and data we collected from our various samples. Short Discussion on the results will be presented at the end of each section. We also give our conclusions in the form of an illustrated model for CNT and CNF growth on stainless steel, which is presented in Section 3.4. Future plans for the project are discussed at the end of this chapter.

3.1 General Characteristics of the CNTs and CNFs

This section will give a general overview of the features that we observed on our samples. The characteristics discussed here are common across all the samples we created.

The first important feature of our CNT samples was their growth direction and height. The nanotubes grow in random orientations, without a preferred alignment. This caused them to spread out along the surface of the material rather than growing upwards. As a result, the nanotubes form a tangled mat or "bramble" rather than an aligned forest. In addition, the height of the growth ranges from 3-7 microns, which is much shorter than what is achievable from silicon-based CNT growth (See Figure 3.5 in Section 3.2). Nanotube lengths are much harder to measure due to the CNTs tangling together, but crude measurements reveal them to be on the order of 10-20 μm.

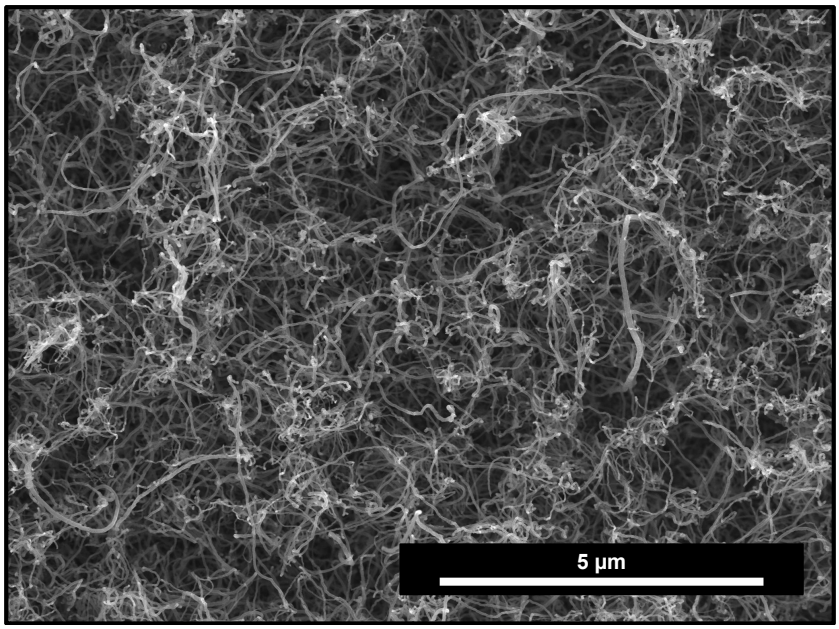

Figure 3.1 Example of CNTs, as grown. Note the tangled growth pattern.

The random orientation and short height of the CNT growth may be due to a low packing density of nanotubes on the surface of the steel. As a result, they are not close enough to force each other upwards into an aligned forest. Alternatively, the nanotube lengths may also be too short for aligned growth to occur. An example of these CNTs can be seen in Figure 3.1.

Another important feature of our nanotubes was their diameters. Fifty CNTs each were randomly selected and measured from samples 16, 20, 21, and 22 (see Appendix A). All the measured diameters are plotted together in Figure 3.2. Across these 4 samples, the nanotubes had an average width of 39 nm, with a standard deviation of 12 nm. This means that most of our nanotubes ranged from 25-50 nm in diameter.

As discussed in Chapter 1, nanotube diameter has a correlation to its structure. MWCNTs tend to have diameters on the order of 10 nm. Shelled CNFs tend to have diameters on the order of 100 nm. Given our measurements, we expected our samples to contain primarily MWCNTs or to be some combination of MWCNTs and CNFs.

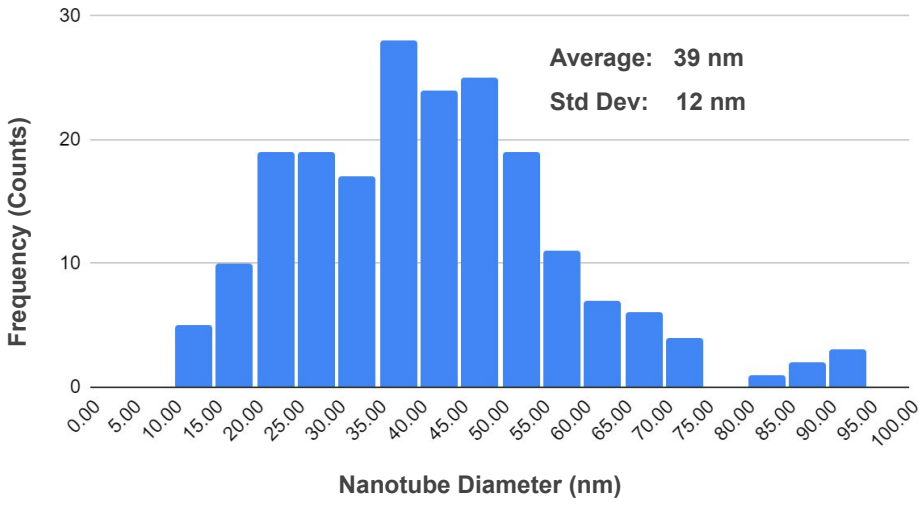

Figure 3.2 Distribution of CNT diameters from our samples. Nanotubes were measured using SEM and ImageJ.

Under SEM imaging, bright particles could often be seen in the tips and throughout the cores of the nanotubes. These cores are likely brighter due to higher density, and later EDX analysis showed that they were iron-rich (see Section 3.3). Similar particles were seen in TEM imaging of the CNTs (see Figure 3.4). These metallic nanoparticles can be seen highlighted in the nanotubes in Figure 3.3.

To confirm the crystal structure of our nanotubes, we scraped CNTs from Sample 20 (see Appendix A) onto a lacey carbon TEM grid. These nanotubes were then imaged in parrallel-beam TEM (see Section 2.). The spacing and parallel direction of lattice fringes in the walls of the CNTs suggest that our CNTs have a structure similar to that of MWCNTs (see Figure 3.4). The nanotubes often contained imperfections that distinguish them from ideal MWCNTs, such as metallic particles in the cores (see Figure 3.4), delamination of the CNT walls, and a thin amorphous carbon layer on the surface (see Figure 3.5).

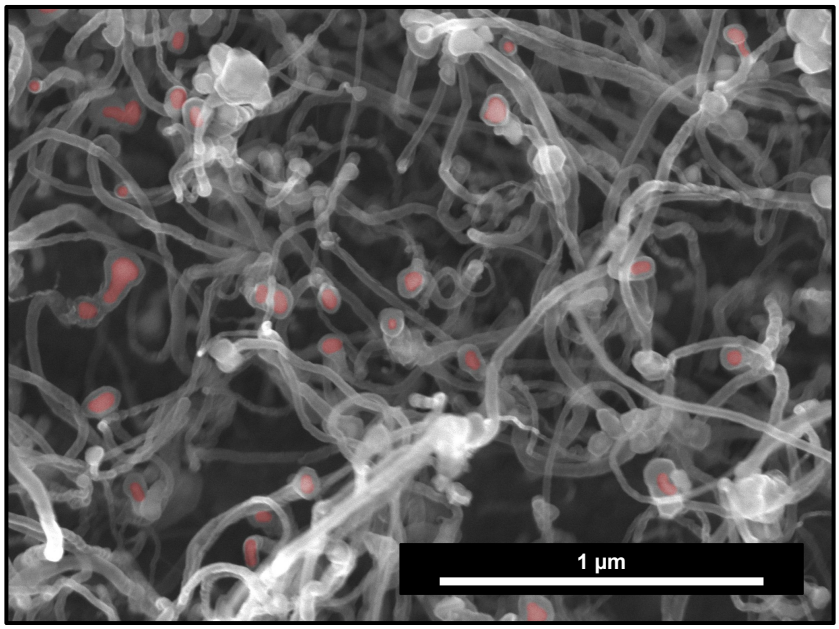

Figure 3.3 Under high magnification, bright particles are seen in the nanotube tips. These have been colored in red to aid the reader.

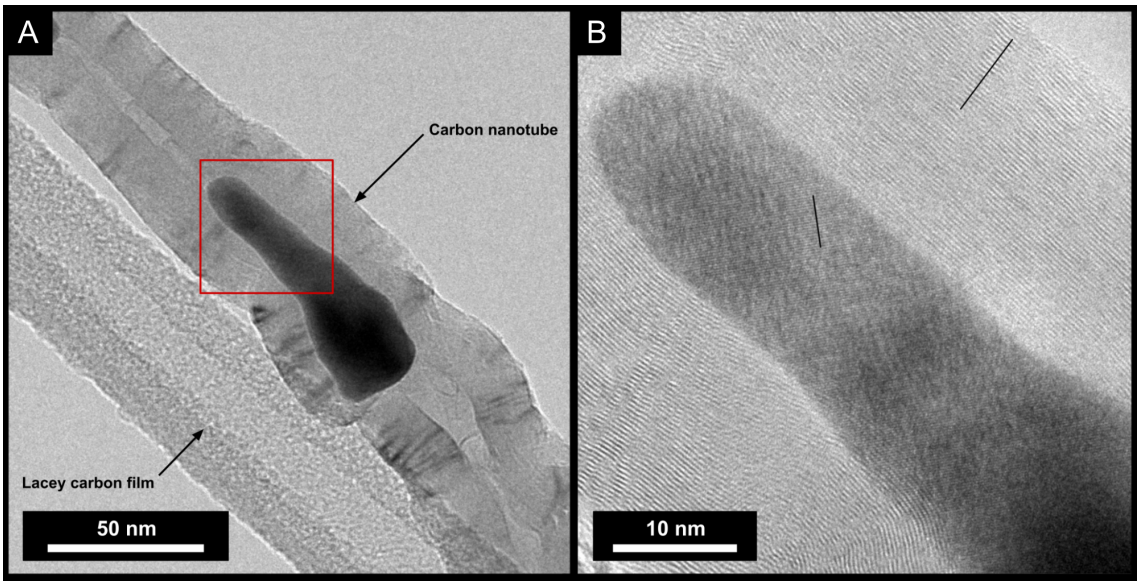

Figure 3.4 A) An isolated CNT from Sample 20 on the lacey carbon support film. The red box shows the magnified region in image B. B) Lattice fringes can be seen in both the metallic nanoparticle and the CNT walls. The spacing of each were measured over 20 bright fringes using the black lines shown. The CNT walls were found to have a spacing of 3.3 angstroms, which matches the spacing for graphene sheets. The nanoparticle had a spacing of 2.0 angstroms, which matches the (110) spacing for BCC iron lattice planes.

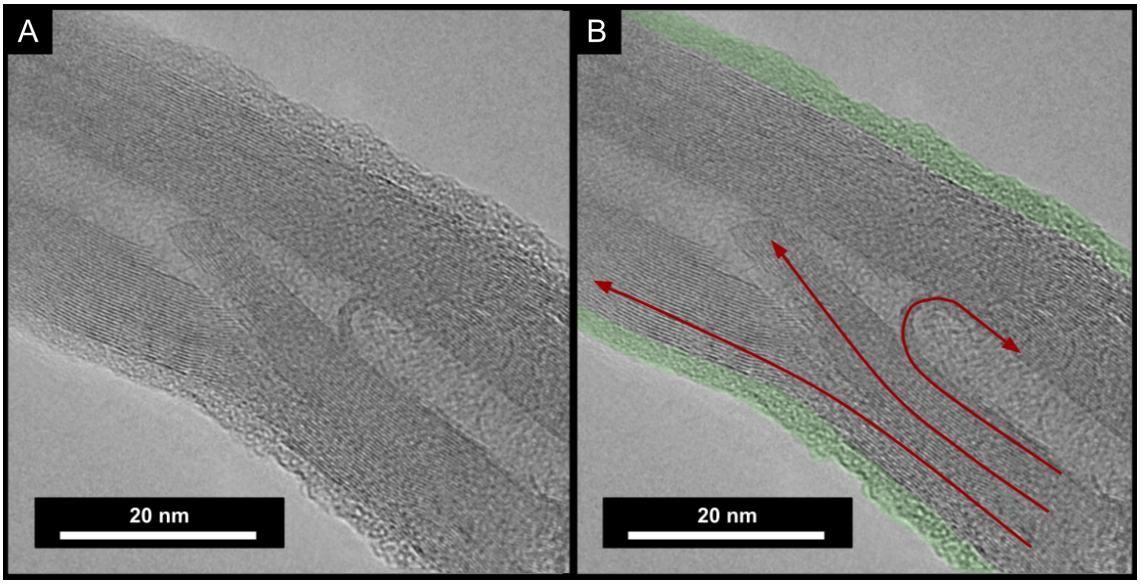

Figure 3.5 Our CNTs contained common imperfections that distinguish them from ideal MWCNTs. Red arrows in image B show the delamination of the graphitic walls into various directions. The crystalline walls of the CNTs were also covered in an amorphous carbon layer, which is highlighted in green in B.

3.2 Effects of Temperature and Hydrogen Reduction

As stated in Section 2.1, all steps of our growth process were performed at a constant temperature. To test the effects of temperature on the CNT growth, samples 16-20 were grown at 800 °C, and samples 21-25 were grown at 700 °C. Each sample also received a different amount of hydrogen reduction between the air heat treatment and ethylene growth steps (See Appendix A for more detail). The effects of this extra hydrogen reduction step and differences between the two temperatures will be discussed in this section.

A plastic stylus was used to gently scrape the CNTs off of the stainless steel substrate to test adhesion. In general, it was found that CNTs grown at 700 °C could be cleanly removed, while CNTs grown at 800 °C were instead knocked over and crushed. This suggests that CNTs may adhere more strongly to the substrate when grown at 800 °C than when grown at 700 °C. A comparison of

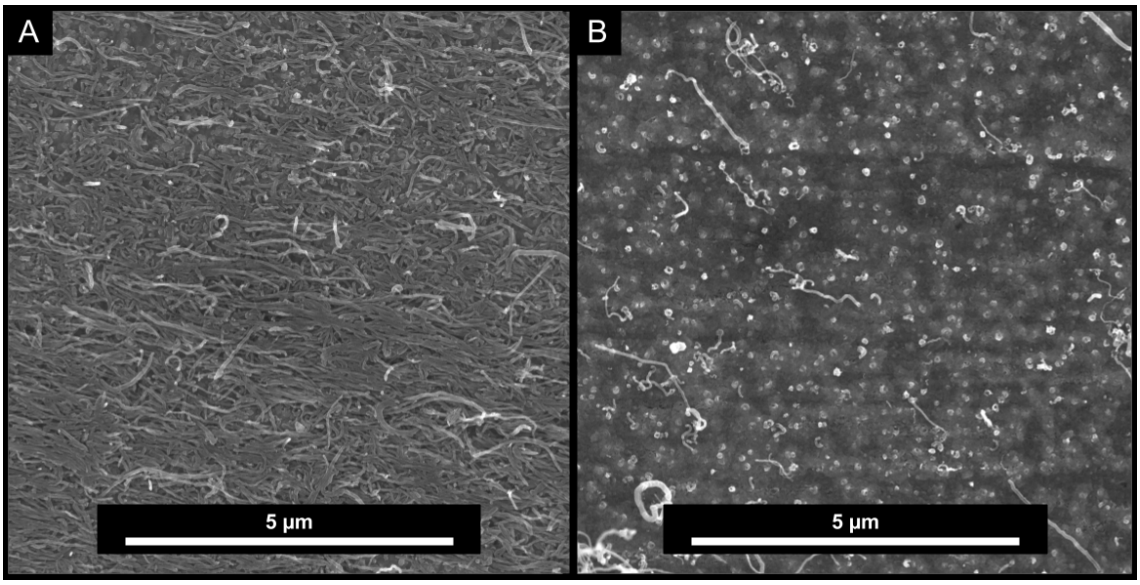

Figure 3.6 A) Scrape test from a sample grown at 800 °C. B) Scrape test from a sample grown at 700 °C. Note that CNTs grown at 800 °C are not removed from the steel and are only knocked down. CNTs grown at 700 °C were cleanly removed.

these two scrape tests can be seen in Figure 3.6.

Performing a hydrogen reduction before growth had very different effects between these two temperatures. At 700 °C, hydrogen reduction led to a small decrease in growth height, but little effect on growth density and tube length. At 800 °C, hydrogen reduction was detrimental to the CNT growth. It led to a swift decrease in growth height and density. After 20 minutes of reduction at 800°C, very few nanotubes remained on the steel surface at all. Images comparing reduction effects on various samples are shown in Figure 3.7. The growth heights of reduced samples are compared in Figure 3.8.

Another interesting effect of hydrogen reduction before growth is how it affects nanotube diameter. Without reduction, CNTs grown at 700 °C are thicker than those grown at 800 °C. Reduction had little effect on the diameter of nanotubes at 800 °C. On the other hand, reduction before growth significantly changed the diameters of nanotubes grown at 700 °C, changing from 55 nm to 31 nm on average. The distributions of these diameters is plotted with their averages in

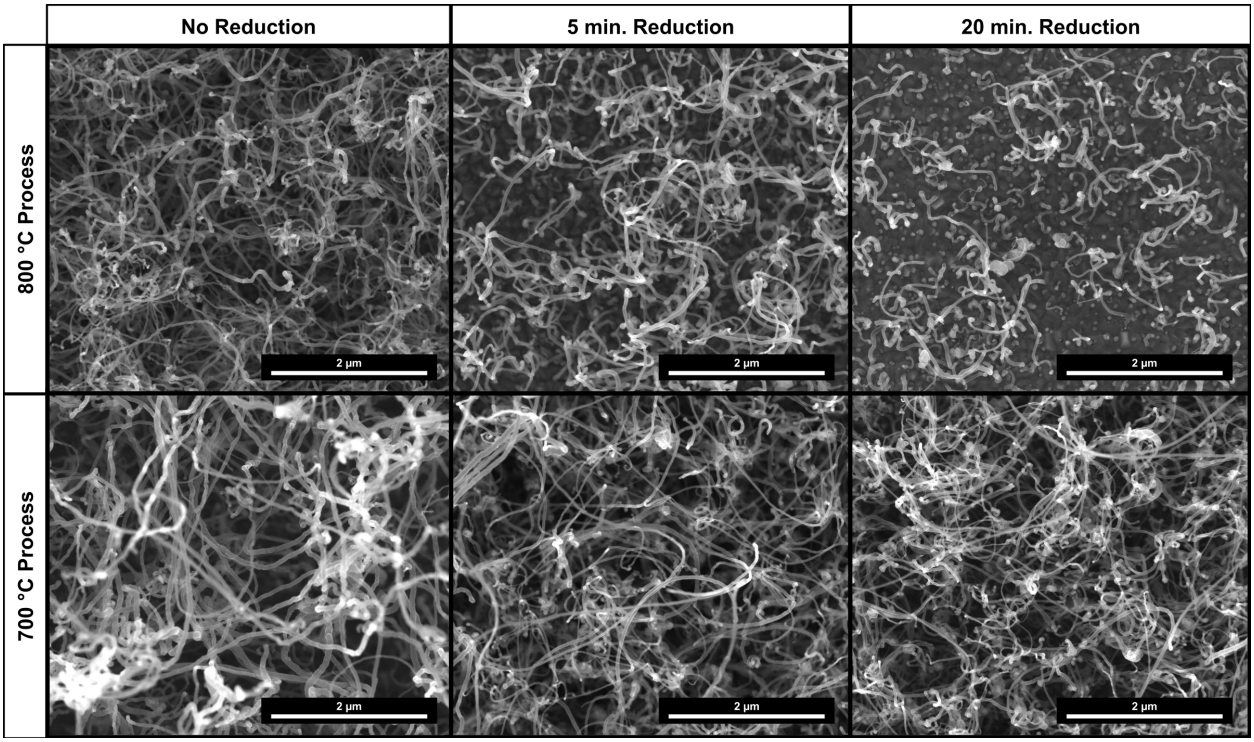

Figure 3.7 Here we compare the effects of pre-growth hydrogen reduction at 800 °C and 700 °C. By comparing the two rows, we can see that reducing the oxides before growth was detrimental to samples grown at 800 °C, while it had a much smaller effect on those grown at 700 °C. For long reductions at 800 °C, small spheres of carbon dot the surface instead of CNTs.

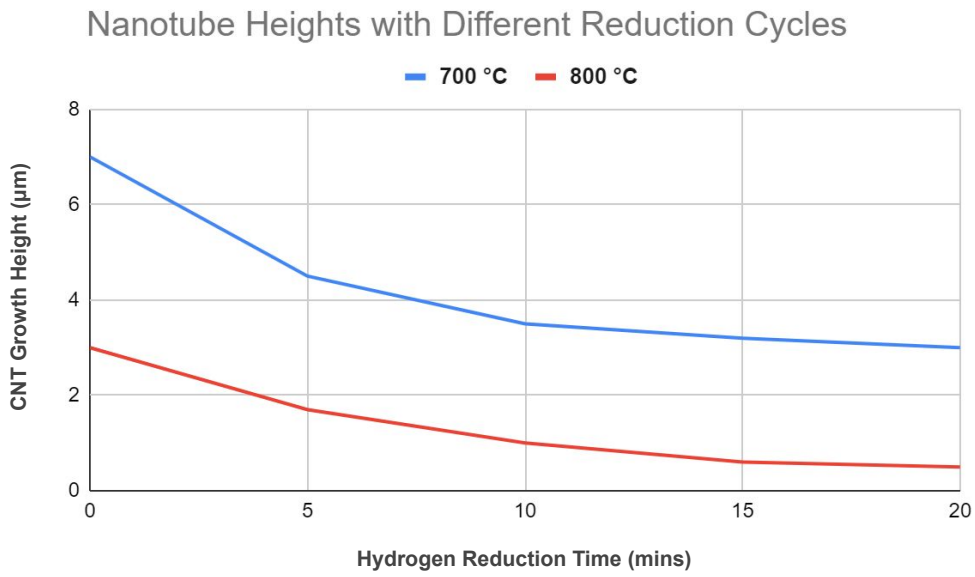

Figure 3.8 Plot of CNT growth height for samples grown with different temperatures and reduction lengths. Samples grown at 700 °C were higher than those grown at 800 °C.

Figure 3.9.

In samples grown at 800 °C with a long hydrogen reduction, it was common to see spherical nodes of amorphous carbon on the surface instead of CNTs (see Figure 3.7). It may be that reduction of the oxides occurs much faster at 800 °C than at 700 °C. By reducing the surface before growth, the oxides may reduce into particles that are too large for CNT growth to be effective. Instead, carbon grows amorphously on the surface due to the high temperature. We predict that this is what causes the reduction step to be so detrimental to CNT growth at 800 °C.

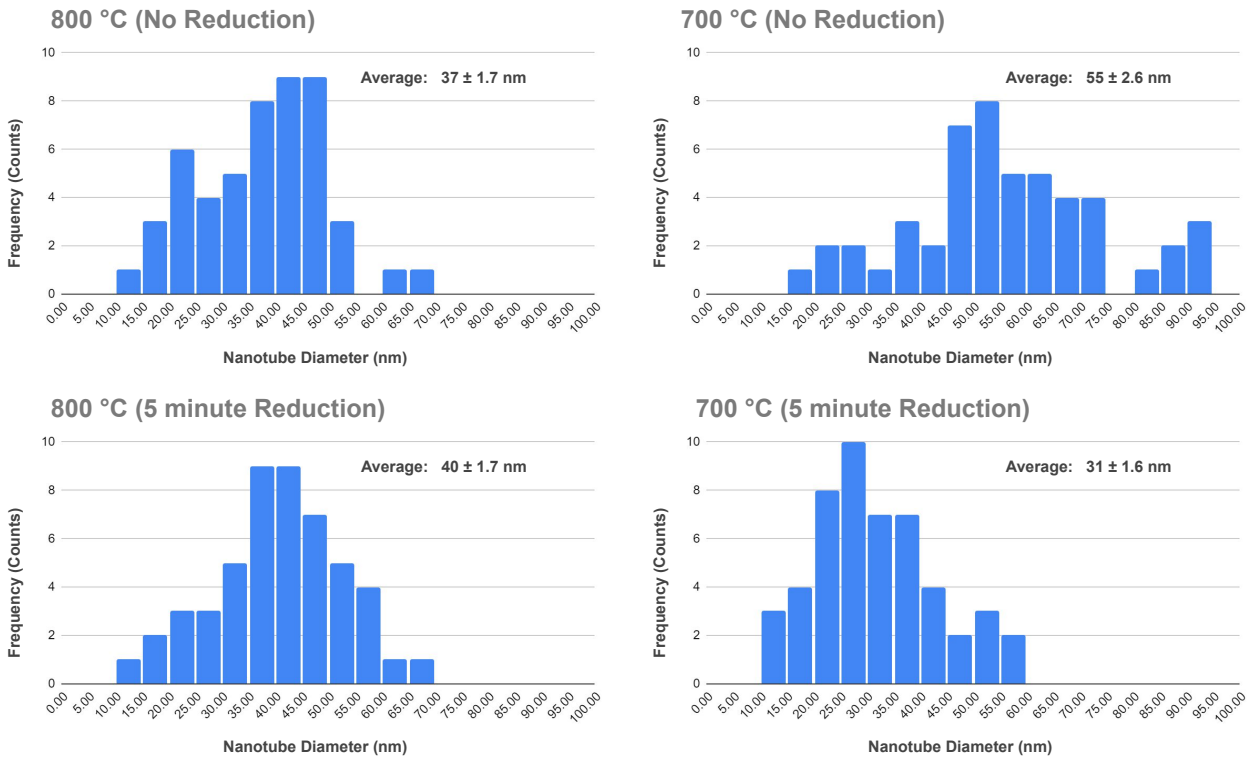

Figure 3.9 These four plots compare the distributions of CNT diameters with and without pre-growth hydrogen reduction at 700 and 800 °C. At 800 °C, hydrogen reduction has little effect on CNT diameter. At 700 °C, hydrogen reduction greatly reduces the average CNT diameter.

3.3 Composition of the Steel Surface and Nanoparticles

This section will present the images and analysis of the TEM lamella cross-sections we took from our samples. We are specifically concerned with how the elemental composition varies near the surface of the steel. We will also be comparing the composition of the various metallic nanoparticles we see throughout our CNTs. As such, the main data presented here was taken with EDX (see Section 2.3). The main cross-sections analyzed were from samples 20 and 26 (see Appendix A).

In STEM, the steel substrate is seen to have an oxide layer on the surface, which was formed during the 4 minute heat treatment before growth. This layer has an average thickness of about 65 nm. EDX analysis on the steel bulk shows that it contains iron, chromium, nickel, and other trace elements; which matches the expected composition for 316L stainless steel. The oxide layer is mostly composed of iron, chromium, and oxygen, but it is notably missing the nickel seen in the bulk. A third distinct layer, which we will call the transition layer, also exists between the oxide and the steel bulk. This region is similar to the bulk steel, but it has a lower Cr/Fe ratio. These three layers can be seen with their EDX spectra in Figure 3.10.

We did EDX analysis on several samples to see how the chemistry of the oxide layer changed over the course of CNT growth, which can be seen in Figure 3.11. The Fe/Cr ratio drops quickly at the start of growth (within the first 20 seconds) and then continues to drop slowly over time. A small amount of nickel is also seen in the oxide before growth, but this is mostly removed in the first 20 seconds of growth. This suggests that iron and nickel are removed from the oxide layer as nanoparticles over the course of the CNT growth process.

In parallel TEM, EDX was taken from a large region of scraped CNTs on a lacy carbon film. This EDX is used to compare the composition of the metallic nanoparticles to that of the original steel in Figure 3.12. The nanoparticles are seen to be primarily iron, with some chromium and nickel mixed in. The Cr/Fe ratio is much lower for the particles than for the steel, suggesting that

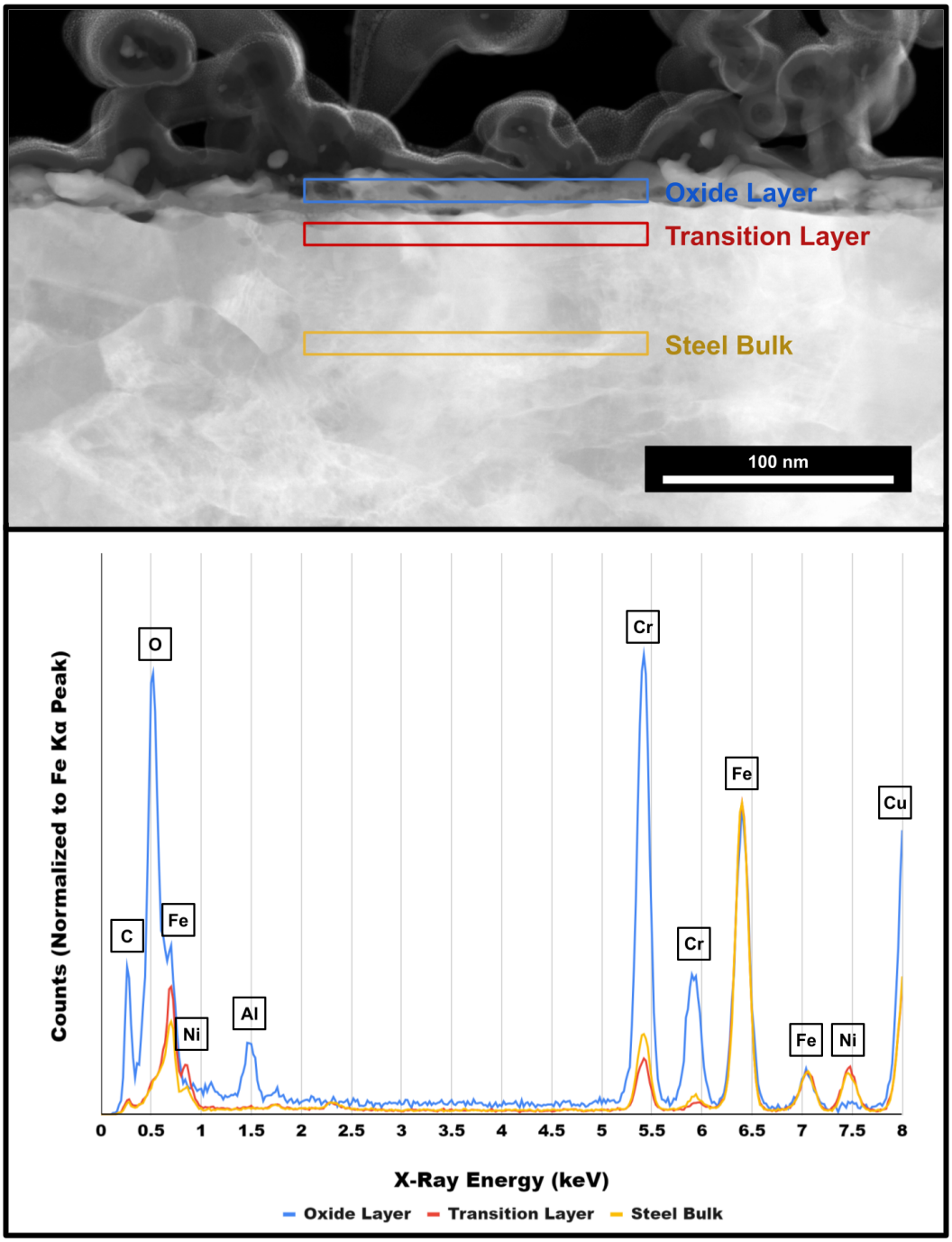

Figure 3.10 The following STEM image was taken of a cross-section from sample 26 (see Appendix A). Three regions were selected for EDX analysis: a part of the oxide, a part of the steel in the bulk, and a transition layer between them. The EDX spectra are shown above. Note that the chromium peak is lower for the transition layer than for the bulk steel, suggesting depletion of chromium from this region.

Fe and Ni reduce out into nanoparticles better than the Cr does.

Regions of a lamella cross-section from sample 20 are shown in Figures 3.13 and 3.14. Metallic particles were seen embedded in the oxide at the base of several CNTs. These CNTs also often had smaller particles in the upper core of the nanotube. EDX analysis of several regions showed that the base particles are more iron-rich than the surrounding oxide. In addition, the upper particles were even more iron-rich than the base particles and also contained nickel. These upper particles closely matched the results from parallel beam EDX (see last paragraph and Figure 3.12). The base particles often looked stretched and torn (see Figures 3.14 and 3.16). It is possible that as the CNT grows, it pulls Fe/Ni-rich particles out of the original base particle, forming the upper particles in the core and tips of the nanotube.

Regions of a lamella cross-section from sample 26 are shown in Figures 3.15 and 3.16. This sample had a CNT growth step of 15 minutes, the longest of any we analyzed. The composition of the reduced base particles and upper particles found in the CNTs themselves matched the results from sample 20. Interestingly, an addition kind of reduced metal was seen in the oxide. These regions matched the Cr/Fe ratio of the surrounding oxide but had much less oxygen. These regions are likely parts of the oxide where all metals were reduced equally. This is different from nanoparticle reduction where iron and nickel seem to reduce preferably to chromium. This suggests that as CNT growth continues, nanoparticle creation slows down and the remaining oxide reduces without creating new iron-rich particles.

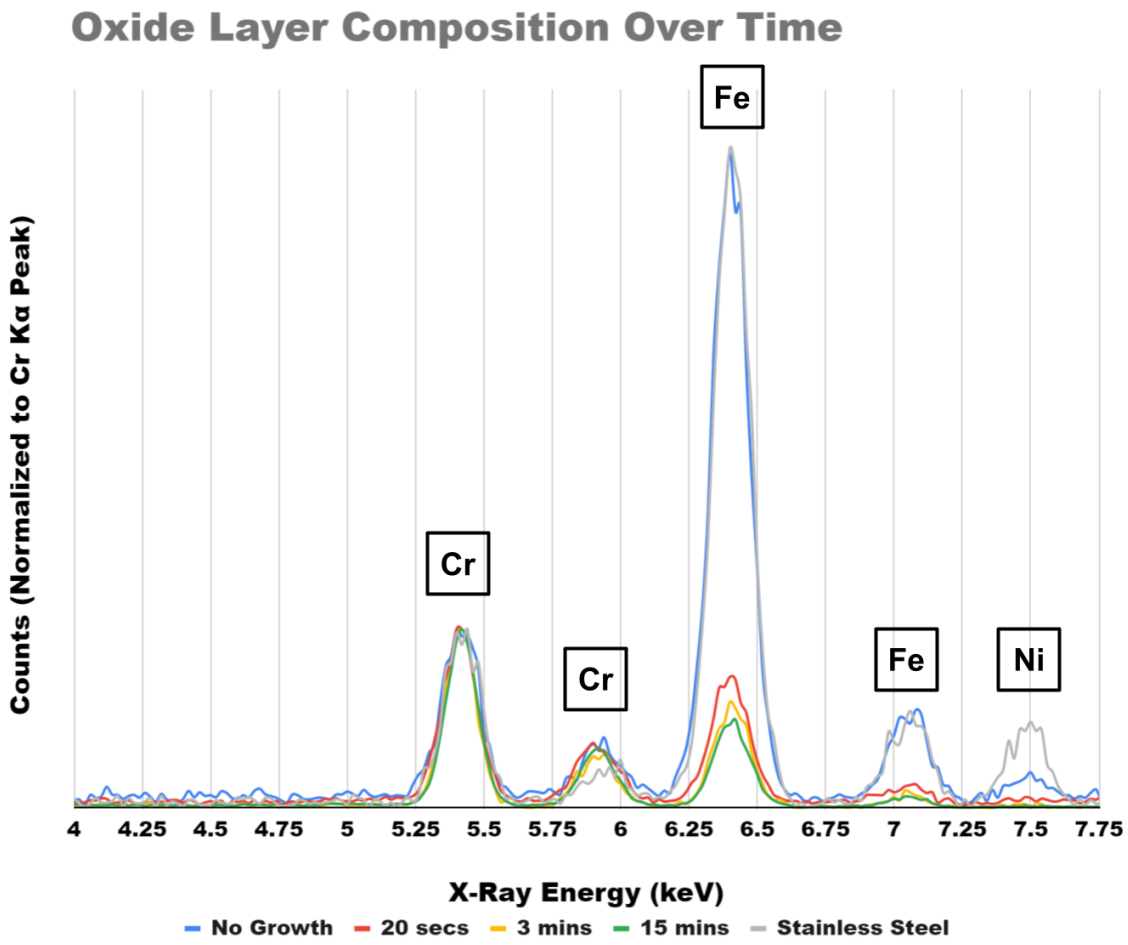

Figure 3.11 The following EDX spectra compares the composition of the oxide layer for samples grown for various lengths of time. The ratios of Fe/Cr match for the oxide and the original steel when no CNT growth is performed. The oxide also contains some Ni before growth, but none afterwards. Note also that the Fe peak drops quickly at first (after only 20 secs. of growth) and then slowly over time.

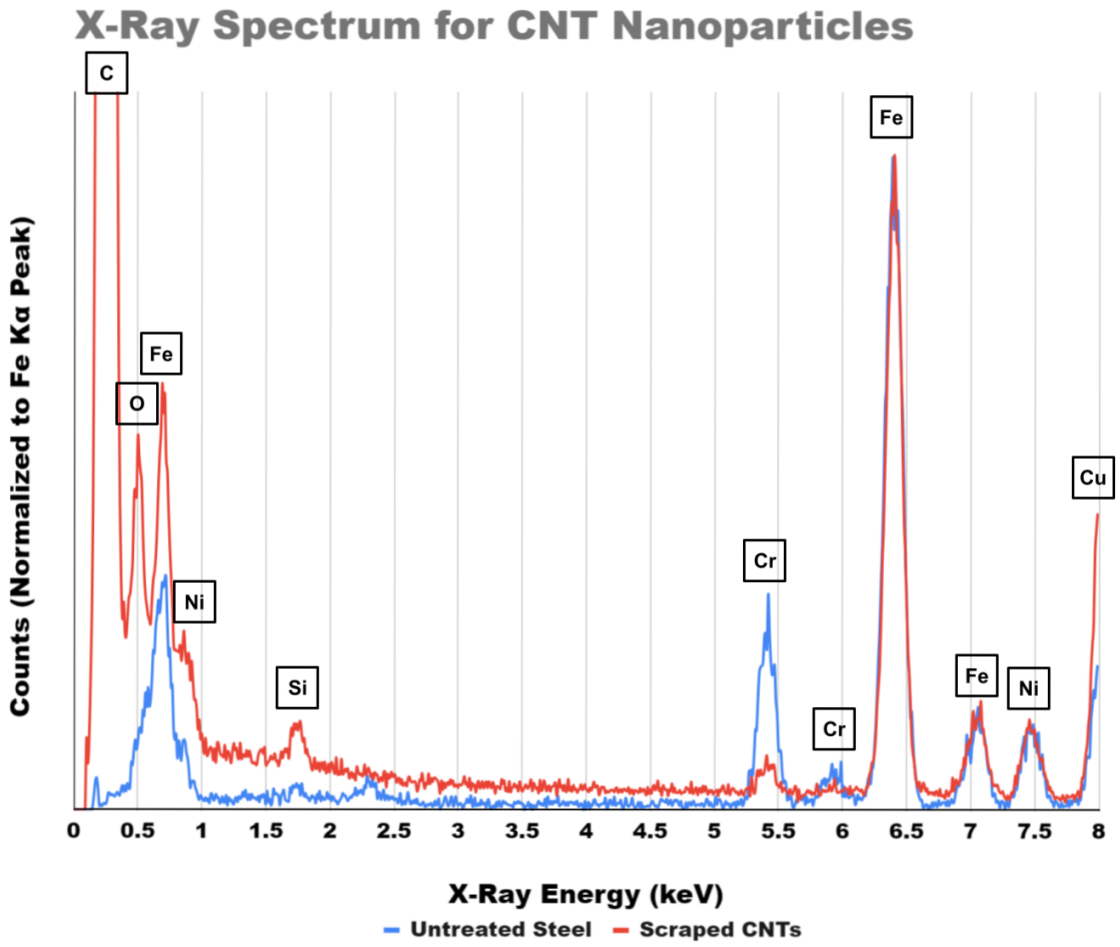

Figure 3.12 The following EDX spectra was taken from a large region of scraped CNTs with metallic nanoparticles in their cores. Although individual nanoparticles are expected to vary from one another in composition, this spectra should capture the general metallic ratios shared by the nanoparticles as a whole. The particles are seen to be mostly Fe, with trace amounts of Ni and Cr. The nanoparticles have a similar Ni/Fe ratio as the steel substrate, but a much lower Cr/Fe ratio.

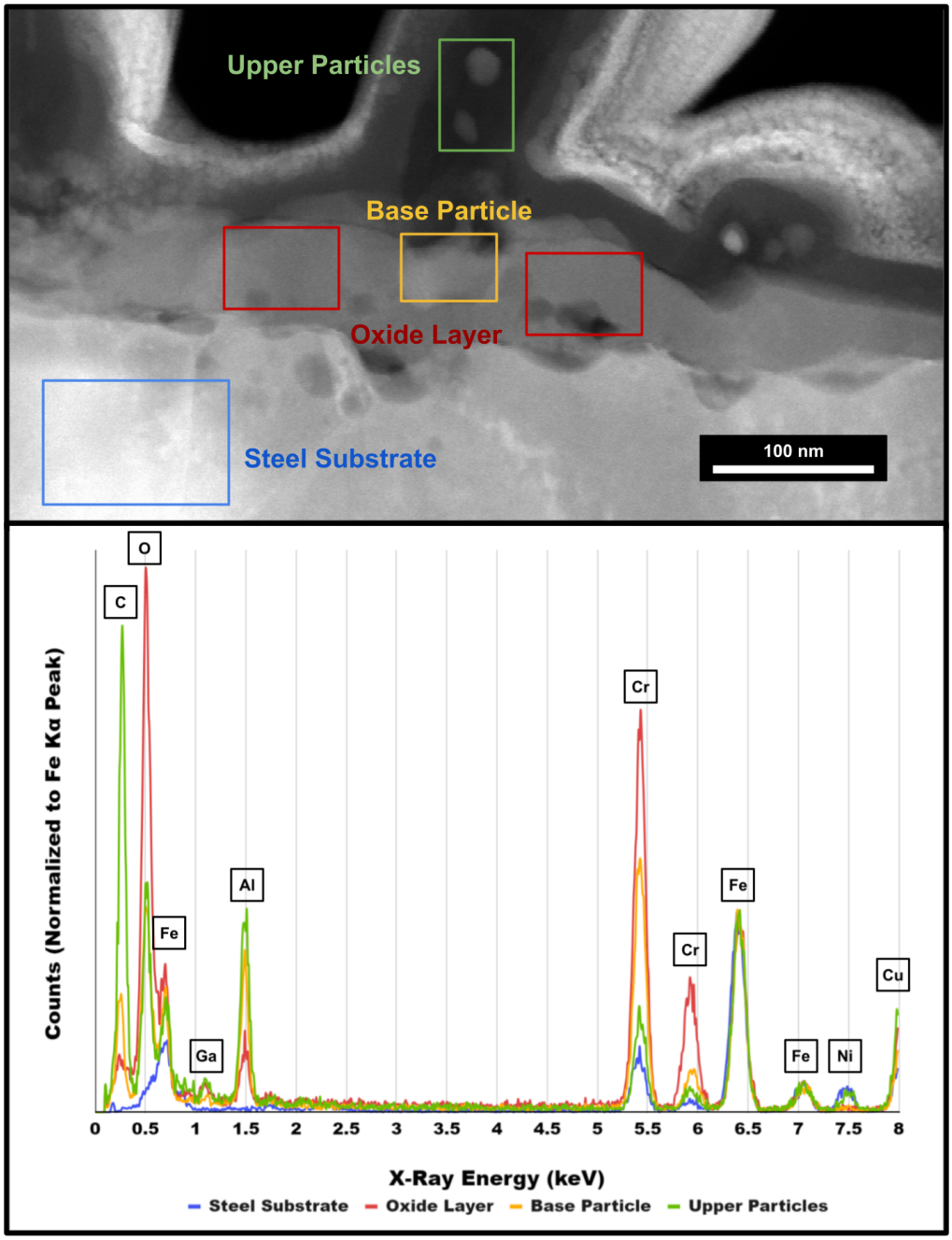

Figure 3.13 The following EDX spectra compares regions of the above cross-section from sample 20. Bright particles are seen both at the base and in the core of the nanotube. The base particle has a lower Cr/Fe ratio than the surrounding oxide, suggesting it is more Fe-rich. The upper particles in the core have an even lower Cr/Fe ratio and also have a substantial Ni peak. From this, we see that the base particles and upper particles are distinct. These results were consistent across several regions (see Figure 3.14).

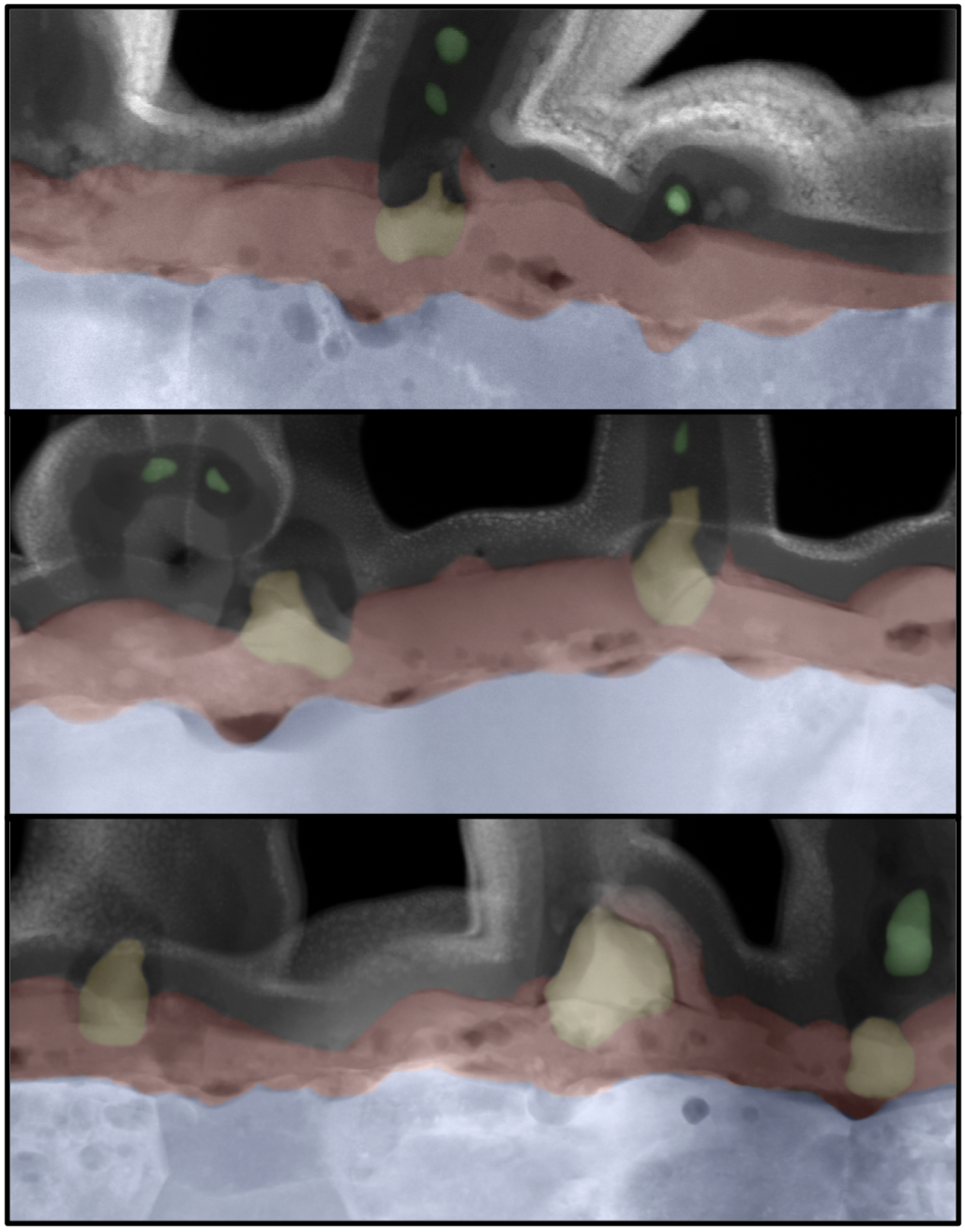

Figure 3.14 These three regions match the results of the EDX shown in Figure 3.13. Different regions have been colorized according to the spectra to better emphasize them. Many of the base particles (yellow) appear stretched and torn. It's possible that the upper particles (green) were pulled out of these base particles.

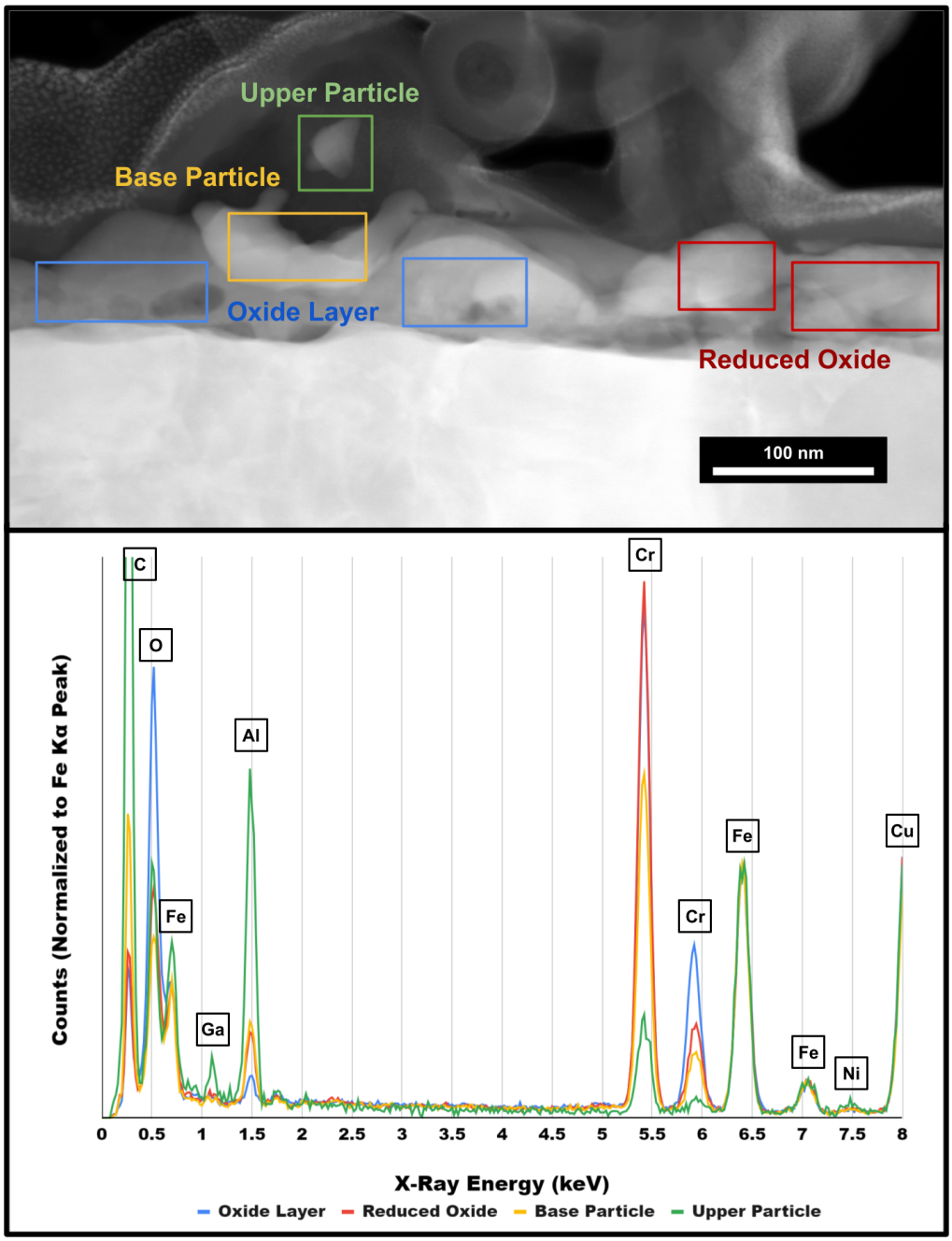

Figure 3.15 The following EDX spectra compares regions of the above cross-section from sample 26. The base and upper particles match the same trends shown in Figure 3.13 In addition, certain regions of the oxide are reduced evenly, such that these regions maintain the same Cr/Fe ratio as the surrounding oxide. This suggests that over long growth periods, the remainder of the oxide reduces without forming Fe-rich nanoparticles. These results were consistent across several regions (see Figure 3.16).

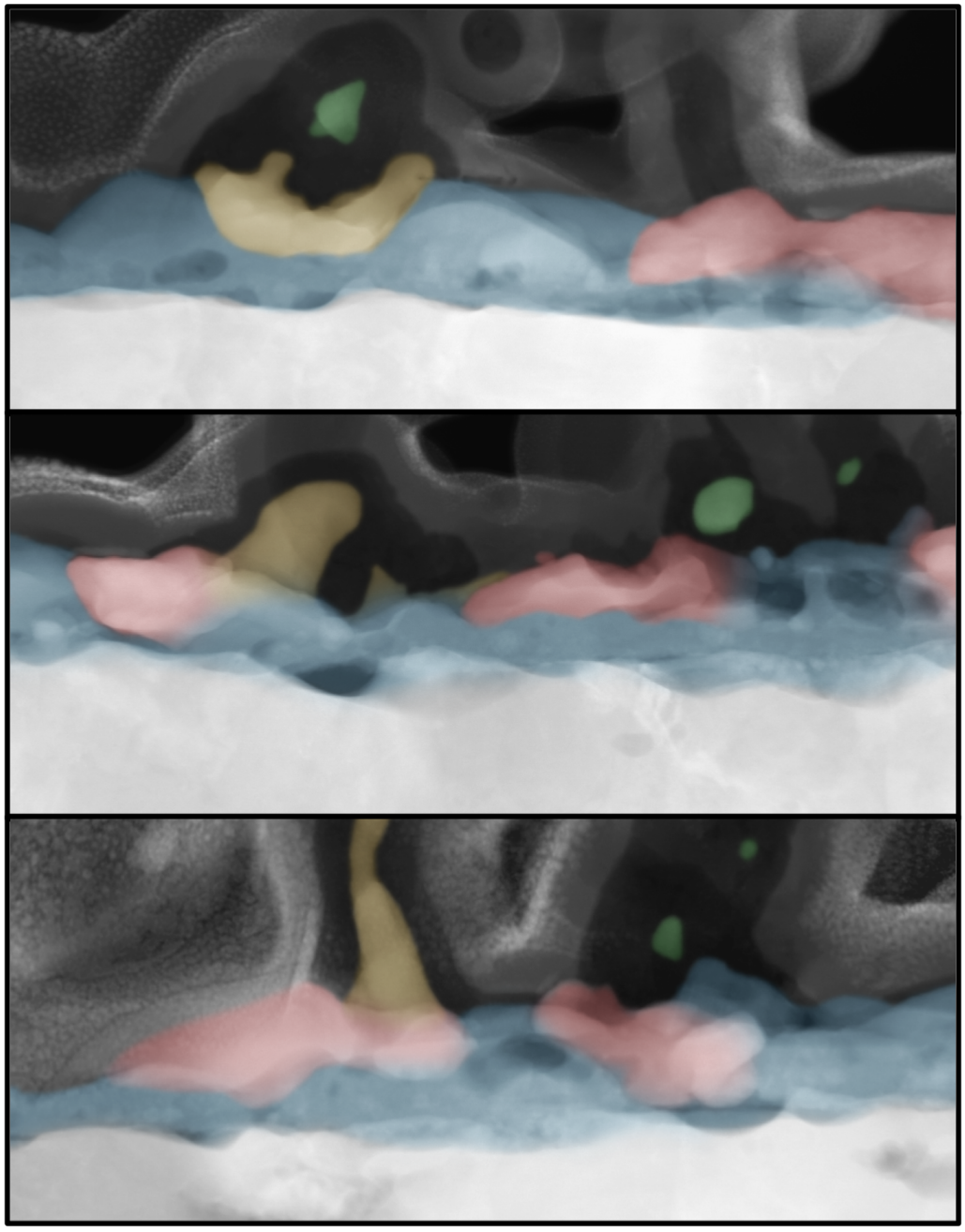

Figure 3.16 These three regions match the results of the EDX shown in Figure 3.15. Different regions have been colorized according to the spectra to better emphasize them. While the base particles (yellow) are always at the base of a CNT, the reduced oxides (red) don't always correlate to a nanotube base. This means they may not act as active catalysts.

3.4 Conclusions: Model of Growth

Putting all of our results together, we have created a model to explain how we believe CNTs grow on stainless steel and how that growth process changes the steel surface. The key results that support this model comes from our EDX analysis from the previous section. Our model is summarized here as a 4 step process. Illustrations of the process are included at the end in Figure 3.11.

3.4.1 Oxidizing Heat Treatment

To prepare the substrate for CNT growth, the stainless steel must first be oxidized. To do this, air is passed over the surface at a high temperature. As the steel oxidizes, metals leave the surface to form a composite oxide layer of iron, chromium, and nickel oxide. This leaves a transition layer between the steel bulk and the oxide that is relatively lower in Cr than the bulk steel underneath.

3.4.2 Oxide Reduction

Before CNTs can begin to grow, metal particles must be reduced out of the oxide layer to act as catalysts. This reduction step can occur with pure hydrogen, but the hydrogen present in the ethylene gas is also sufficient to reduce the oxides. Iron and nickel reduce out of the oxide layer faster than the chromium, creating Fe/Ni-rich nanoparticles that will catalyze CNT growth. If reduction occurs for too long before CNT growth begins, the particles that reduce out of the oxide may become too large for ideal growth. The majority of nanoparticle creation happens quickly, dropping the Fe/Ni content of the oxide and leaving it Cr-rich.

3.4.3 Short CNT growth

Ethylene gas or other hydrocarbons are used as the precursor for CNT growth. At the high growth temperatures, the C_2H_4 breaks down into hydrogen and carbon. Metallic nanoparticles on the oxide

surface absorb carbon and catalyze CNT growth. As the nanotubes grow, the particles are stretched and broken, pulling the more Fe/Ni-rich parts into the tips and cores of the CNTs. A portion of the original particle is left behind at the base.

3.4.4 Long CNT growth

The remaining oxide continues to reduce more evenly, slowing nanoparticle production. Eventually, all the oxygen is removed from the oxide and no more nanoparticles can be formed. At this stage, we suspect that no new nanotubes can be grown. In addition, we suspect that the isolated base particles may cease to be active catalysts, stopping the growth of existing CNTs. What is left on the surface is an irregular alloy layer of Cr and Fe and a depleted steel layer underneath that is poor in Cr. As a result, the surface of the steel has a different composition than the stainless alloy in the bulk.

3.5 Future Work

It is important to note that, although this model was made using all of the data and observations we have shared in this chapter, it serves only as an early hypothesis. It must be more thoroughly tested before it can be proven. We intend to continue developing experiments and gathering data to test this model in the future work of this project.

As it currently stands, we have only analyzed two of our samples with STEM and EDX. If we want to better understand how factors like temperature and hydrogen reduction affect the chemistry of the steel surface, we will need to create and analyze lamella cross-sections of our other samples.

The longest grown sample that we have analyzed was a 15 minute ethylene exposure. Given that oxides are still present at this time, growth should be able to continue for a longer period. We would like to analyze longer grown samples, such as those with a 30 minute or 60 minute ethylene

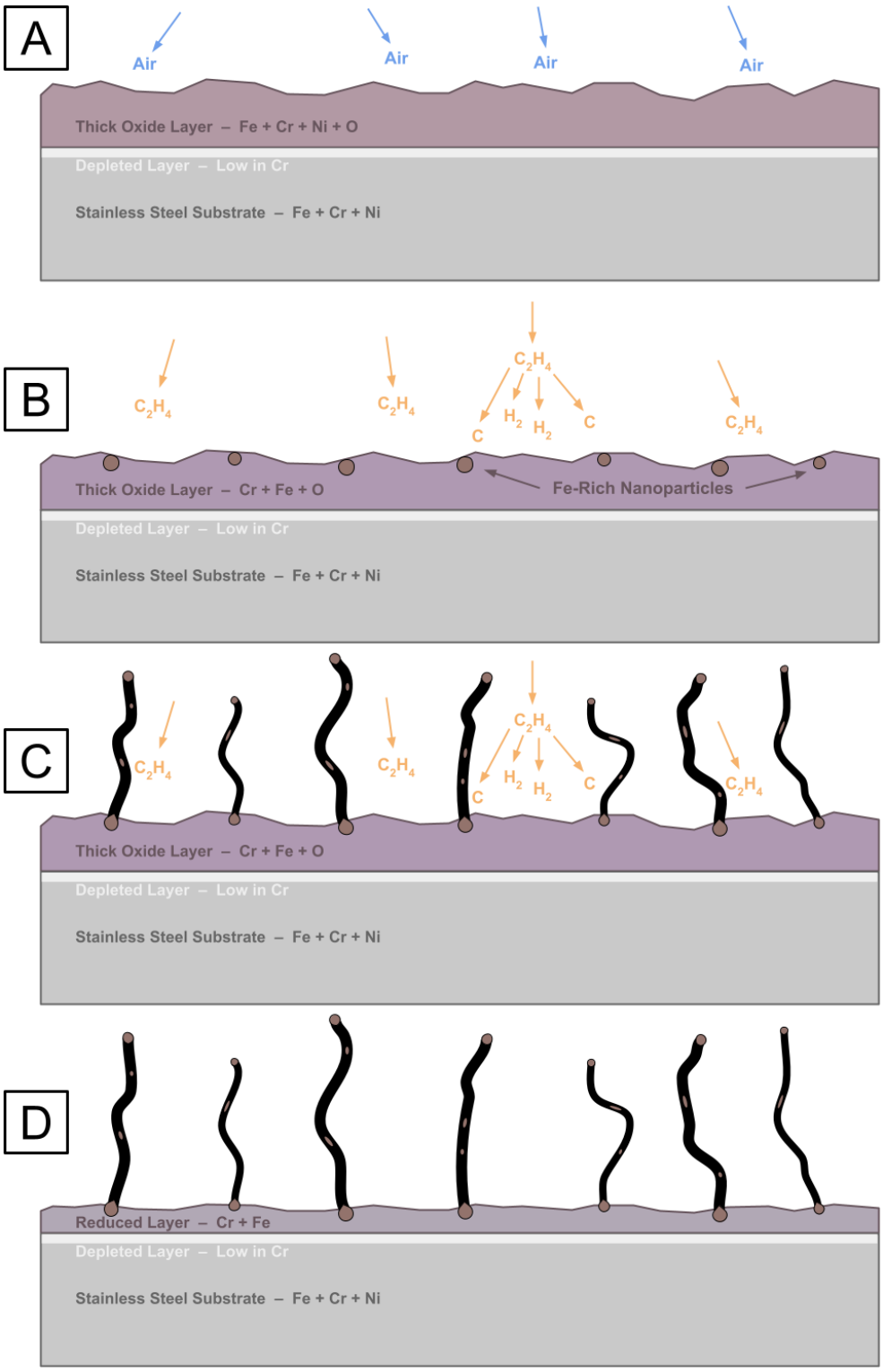

Figure 3.17 Illustrated model for CNT growth on stainless steel.

exposures, in order to see how the surface chemistry looks when all oxides have been reduced. It would also allow us to see if nanotubes continue to grow or not after all oxides have been removed.

Temperature was seen to affect various parts of the CNT growth process. Nanotubes grown at 700 °C have wider diameters than those grown at 800 °C. In addition, reducing the oxides before growth was detrimental at 800 °C, but not at 700 °C. Reducing before growth also decreased the nanotube diameter for tubes grown at 700 °C, but not for those grown at 800 °C. As of now, we don't understand why these differences exist. Creating STEM lamella for EDX analysis from reduced samples and samples grown at 700 °C would help us see if the surface chemistry changes with temperature. We can also grow and analyze samples at other temperatures, such as 600 °C or 750 °C, to have more data points from which to find correlations.

In previous studies on biocompatibility, the CNT samples were grown for long periods of time and were carbon infiltrated. It is likely that this caused the entire oxide surface to be reduced, making the steel prone to corrosion. It is possible that by growing CNTs for a short period to leave a Cr-rich oxide intact, the surface may remain corrosion resistant. As a result, we would like to test the corrosion resistance and biocompatibility of short CNT growth samples.

In general, there are still a lot of questions we would love to answer, and I am certain that this project still has more for us to find; and as we refine our model, we may be able to find better ways to maximize CNT yield and find applications for this unique substrate in CNT production.

Appendix A: Sample Key

Sample No.	Temperature	Heat Treatment (Air)	Reduction (H_2)	Growth (C_2H_4)
Note: Samples 1-15 are excluded here due to the poor grade of the steel substrate used				
16	800 °C	4 mins	5 mins	3 mins
17	800 °C	4 mins	10 mins	3 mins
18	800 °C	4 mins	15 mins	3 mins
19	800 °C	4 mins	20 mins	3 mins
20	800 °C	4 mins	—	3 mins
21	700 °C	4 mins	—	3 mins
22	700 °C	4 mins	5 mins	3 mins
23	700 °C	4 mins	10 mins	3 mins
24	700 °C	4 mins	15 mins	3 mins
25	700 °C	4 mins	20 mins	3 mins
26	800 °C	4 mins	—	15 mins
27	700 °C	4 mins	—	15 mins
28	700 °C	4 mins	60 mins	3 mins
29	800 °C	4 mins	1 min	3 mins
30	800 °C	4 mins	—	1 min
31	800 °C	4 mins	—	20 secs
32	800 °C	4 mins	—	—

Bibliography

[1] A. Hassan, H. Elkady, and I. G. Shaaban, "Effect of Adding Carbon Nanotubes on Corrosion Rates and Steel-Concrete Bond," Scientific Reports 9 (2019).

[2] S. Mori and M. Suzuki, "Non-Catalytic, Low-Temperature Synthesis of Carbon Nanofibers by Plasma-Enhanced Chemical Vapor Deposition," in *Nanofibers* (IntechOpen, Rijeka, 2010), Chap. 15.

[3] D. N. Hutchison, N. B. Morrill, Q. Aten, B. W. Turner, B. D. Jensen, L. L. Howell, R. R. Vanfleet, and R. C. Davis, "Carbon Nanotubes as a Framework for High-Aspect-Ratio MEMS Fabrication," Journal of Microelectromechanical Systems **19,** 75–82 (2010).

[4] U. Pakdee, S. Chiangga, S. Suwannatus, and P. Limsuwan, "Growth of MWCNTs on Flexible Stainless Steels without Additional Catalysts," Journal of Nanomaterials 84 (2017).

[5] L. Camilli, M. Scarselli, S. Del Gobbo, P. Castrucci, F. Nanni, E. Gautron, S. Lefrant, and M. De Crescenzi, "The synthesis and characterization of carbon nanotubes grown by chemical vapor deposition using a stainless steel catalyst," Carbon **49,** 3307–3315 (2011).

[6] L. Camilli *et al.*, "High coercivity of iron-filled carbon nanotubes synthesized on austenitic stainless steel," Carbon **50,** 718–721 (2012).

[7] C. Zhuo, X. Wang, W. Nowak, and Y. A. Levendis, "Oxidative heat treatment of 316L stainless steel for effective catalytic growth of carbon nanotubes," Applied Surface Science **313,** 227–236 (2014).

[8] S. Pattinson, V. Balakrishnan, D. Zakharov, J. Li, E. Stach, and A. J. Hart, "Mechanism and Enhanced Yield of Carbon Nanotube Growth on Stainless Steel by Oxygen-Induced Surface Reconstruction," Chemistry of Materials **27,** 932–937 (2015).

[9] X. Ke, S. Bals, A. Romo Negreira, T. Hantschel, H. Bender, and G. Van Tendeloo, "TEM Sample Preparation by FIB for Carbon Nanotube Interconnects," Ultramicroscopy **109,** 1353–1359 (2009).

[10] S. R. Morco, "Characterizing Bacterial Resistance and Microstructure-Related Properties of Carbon-Infiltrated Carbon Nanotube Surface Coatings with Applications in Medical Devices," Theses and Dissertations (Brigham Young University, Provo, UT, 2021).

[11] S. C. Voss, "Effects of Carbon-Infiltrated Carbon Nanotube Growth on the Biocompatibility of 316L Stainless Steel," Theses and Dissertations (Brigham Young University, Provo, UT, 2021).

[12] M. Manwaring, "Surface Modification of 316L Stainless Steel for Carbon Nanotube Growth," Theses and Dissertations (Brigham Young University, Provo, UT, 2021).

Index

carbon nanofibers (CNF), 1, 15
carbon nanotubes, multi-walled (MWCNT), 1, 15
carbon nanotubes, single-walled (SWCNT), 1
chemical vapor deposition (CVD), 1, 8

energy dispersive X-ray spectroscopy (EDX), 12, 23

focused ion beam (FIB), 11

hydrogen reduction, 9, 18, 32

iron nanoparticles, 3, 16, 23, 25

nanotube diameter, 9, 15, 21
nanotube growth height, 9, 19

oxide layer, 5, 23, 32
oxidizing heat treatment, 5, 8, 32

scanning transmission electron microscope (STEM), 12, 23
steel bulk, 23
substrate adhesion, 9, 19
surface modification, 23, 33